 CMES, vol.94, no.5, pp.421-458, 2013

On Static Analysis of Composite Plane State Structures via GDQFEM and Cell Method

E. Viola[1], F. Tornabene[1] E. Ferretti[1] and N. Fantuzzi[1]

Abstract: In this paper, an advanced version of the classic GDQ method, called the Generalized Differential Quadrature Finite Element Method (GDQFEM) is formulated to solve plate elastic problems with inclusions. The GDQFEM is compared with Cell Method (CM) and Finite Element Method (FEM). In particular, stress and strain results at fiber/matrix interface of dissimilar materials are provided. The GDQFEM is based on the classic Generalized Differential Quadrature (GDQ) technique that is applied upon each sub-domain, or element, into which the problem domain is divided. When the physical domain is not regular, the mapping technique is used to transform the fundamental system of equations and all the compatibility conditions. A differential problem defined on the regular master element in the computational domain is turned into an algebraic system. With respect to the very well-known Finite Element Method (FEM), the GDQFEM is based on a different approach: the direct derivative calculation is performed by using the GDQ rule. The imposition of the compatibility conditions between two boundaries are also used in the CM for solving contact problems. Since the GDQFEM is a higher-order tool connected with the resolution of the strong formulation of the system of equations, the compatibility conditions must be applied at each disconnection in order to capture the discontinuity between two boundaries, without losing accuracy. A comparison between GDQFEM, CM and FEM is presented and very good agreement is observed.

Keywords: Generalized Differential Quadrature Finite Element Method, Inclusion problem, Boundary Value Problem, Cell Method.

1 Introduction

It is well-known in literature that the elastic behaviour of composite solids such as particle and fiber-reinforced composites can be described as a Boundary Value

[1] DICAM Department, University of Bologna, Italy.

Problem (BVP), that is an elliptic system of equations containing non-homogeneous conditions. When discontinuous coefficients, such as different elastic moduli, are introduced in the physical model, finite jumps in terms of displacements and stresses occur across the interface. The BVPs presented in this paper are common in mechanics of two dimensional solids when a certain material is embedded into a matrix with different mechanical properties. There are several computational methodologies that study the present problem [Tonti (2001); Ferretti (2001, 2003, 2004a,b,c, 2005, 2009, 2012, 2014, 2013a,b); Ferretti, Casadio, and Di Leo (2008); Wu, Park, and Chen (2011); Wu, Guo, and Askari (2013)]. Moreover, many scientists have tried new ways for analysing elastic structures using several numerical procedures [Li, Shen, Han, and Atluri (2003); Sladek, Sladek, and Atluri (2004); Han, Liu, Rajendran, and Atluri (2006); Li and Atluri (2008a,b)]. In addition, the computational mechanics of micro and macro composites also lies in the following works [Dong and Atluri (2012b,a,c,d, 2013)]. Furthermore, such problems are solved using the Generalized Differential Quadrature Finite Element Method (GDQFEM). This numerical technique is an advanced version of the well-known Generalized Differential Quadrature (GDQ) method, which has been increasingly developed over the years [Artioli, Gould, and Viola (2005); Tornabene and Ceruti (2013a,b); Tornabene, Fantuzzi, Viola, and Carrera (2014)]. Compared to the Finite Element Method (FEM), GDQ yields very accurate results by using a very small amount of nodal points [Tornabene (2009, 2011a,b,c); Viola, Dilena, and Tornabene (2007); Viola, Tornabene, and Fantuzzi (2013a,c)]. However, several computational difficulties arise when GDQ is applied to plane elastic problems where discontinuities are present, such as geometry distortion and mechanical inhomogeneities. Generally a finite stress jump occurs when a BVP is considered. It has been demonstrated mathematically that a discontinuity must be treated with a higher-order numerical scheme [Sod (1978)]. It is worth reminding that the phrase "differential quadrature" is equivalent to Lagrange interpolation and differentiation using Lagrange polynomials [Shu (2000); Tornabene, Marzani, Viola, and Elishakoff (2010); Tornabene (2012)]. In short, it is a higher-order numerical scheme that can be differentiable for many orders and can be applied on regular domains, such as squares and rectangles, as well as curvilinear orthogonal coordinate systems [Tornabene, Liverani, and Caligiana (2011, 2012b,c,a); Tornabene and Viola (2007, 2008, 2009a,b, 2013); Tornabene and Reddy (2013)]. In the present paper, an advanced version of the classic GDQ method is formulated to solve plane elastic problems with inclusions. The given physical system is divided into several sub-domains (or elements) in order to capture the mechanical and geometrical discontinuities of the problem under consideration. The BVP is solved considering the boundary of each sub-domain at the interface of two different materials and the computational discontinuity is transformed into a proper imposition of compatibil-

ity condition at the interface itself. In detail, the continuity condition is made of two relationships. The first condition imposes the equality of the displacements between the two adjacent edges, whereas the second one enforces the equality of stresses between neighboring sides. Furthermore, it has been proven in literature [Chen (1999a,b, 2000, 2003)] that the boundary condition treatment is a key point of GDQFEM. Thus, numerical accuracy can change significantly when the implementation of boundary conditions is modified.

In conclusion, it should be mentioned that irregular GDQ implementation [Bert and Malik (1996)] has been introduced in order to solve structures that did not have a regular shape. This occurs especially in civil, mechanical and aerospace engineering applications.

2 Plane elasticity

In the theory of elasticity, stress and strain components are generally described by three dimensional tensors but, for some cases, when the length of the structure is much smaller than the other two dimensions [Timoshenko (1934)] they may be assumed as two dimensional. For the plane strain conditions, the strain associated with the structure thickness ε_z and the shear strains γ_{xz}, γ_{yz} are equal to zero. The kinematic relations for the plane strain problem can be written in matrix form as

$$\boldsymbol{\varepsilon} = \mathbf{D}\mathbf{u}, \quad \text{for} \quad \mathbf{D} = \begin{bmatrix} \frac{\partial}{\partial x} & 0 \\ 0 & \frac{\partial}{\partial y} \\ \frac{\partial}{\partial y} & \frac{\partial}{\partial x} \end{bmatrix} \tag{1}$$

where the strain vector is $\boldsymbol{\varepsilon} = \begin{bmatrix} \varepsilon_x & \varepsilon_y & \gamma_{xy} \end{bmatrix}^T$ and the displacement vector is $\mathbf{u} = \begin{bmatrix} u & v \end{bmatrix}^T$. The constitutive relationships assume the aspect

$$\boldsymbol{\sigma} = \mathbf{C}\boldsymbol{\varepsilon}, \quad \text{for} \quad \mathbf{C} = \begin{bmatrix} 2G+\lambda & \lambda & 0 \\ \lambda & 2G+\lambda & 0 \\ 0 & 0 & G \end{bmatrix} \tag{2}$$

where the stress vector is $\boldsymbol{\sigma} = \begin{bmatrix} \sigma_x & \sigma_y & \tau_{xy} \end{bmatrix}^T$. It should be noted that, for the plane strain condition at issue, $\sigma_z = \lambda\,(\varepsilon_x + \varepsilon_y)$. In fact, the stress corresponding to a plane strain condition does not form a plane stress tensor. Since in the following numerical examples the elastic modulus E and the Poisson's ratio ν are used, the equation of transformation for the elastic constants must be introduced [Timoshenko (1934)], $G = \frac{E}{2(1+\nu)}$, $\lambda = \frac{\nu E}{(1+\nu)(1-2\nu)}$.

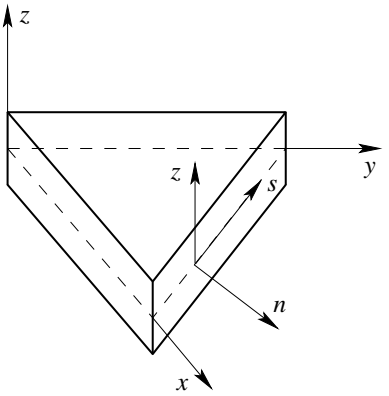

Figure 1: Local reference system for a generic inclined boundary.

Finally, the equilibrium equations for an elastic plane problem take the form

$$\mathbf{D}^{*}\boldsymbol{\sigma}+\mathbf{f}=\mathbf{0}, \quad \text{for} \quad \mathbf{D}^{*}=\begin{bmatrix} \frac{\partial}{\partial x} & 0 & \frac{\partial}{\partial y} \\ 0 & \frac{\partial}{\partial y} & \frac{\partial}{\partial x} \end{bmatrix} \tag{3}$$

where the body force vector is defined as $\mathbf{f}=\begin{bmatrix} f_x & f_y \end{bmatrix}^T$. In conclusion, substituting the kinematic equations Eq. 1 in the constitutive ones Eq. 2 and the results in the equilibrium equations Eq. 3, the fundamental system of equations for the static case is found $\mathbf{D}^{*}\mathbf{C}\mathbf{D}\mathbf{u}+\mathbf{f}=\mathbf{0}$ or $\mathbf{L}\mathbf{u}+\mathbf{f}=0$, where $\mathbf{L}=\mathbf{D}^{*}\mathbf{C}\mathbf{D}$ is also termed the fundamental operator. The dynamic case can be obtained from the static one by adding the inertia forces $\mathbf{f}_I=\begin{bmatrix} \rho\ddot{u} & \rho\ddot{v} \end{bmatrix}^T$

$$\mathbf{L}\mathbf{u}+\mathbf{f}=\mathbf{f}_I \tag{4}$$

The partial differential system of equations summarized in Eq. 4 can be solved only when proper boundary conditions are imposed on the domain boundaries. In general, as it is well-known, two types of boundary conditions can be enforced in order to solve a differential system of equations: a Dirichlet type, $\mathbf{u}=\bar{\mathbf{u}}$, and a Neumann type $\frac{\partial \mathbf{u}}{\partial \mathbf{n}}=\mathbf{q}$. The first conditions are referred to the displacements and are called kinematic boundary conditions. The second conditions involve the displacement vector derivatives and they are known as static boundary conditions. In particular, $\bar{\mathbf{u}}$ denotes certain fixed boundary displacements that are usually equal to zero for a fixed edge, $\bar{\mathbf{u}}=\mathbf{0}$. The vector $\mathbf{q}$ stands for the flux vector and in the present paper it gathers the external applied loads to the given physical domain. It should be noted that static boundary conditions are very important, because they also are

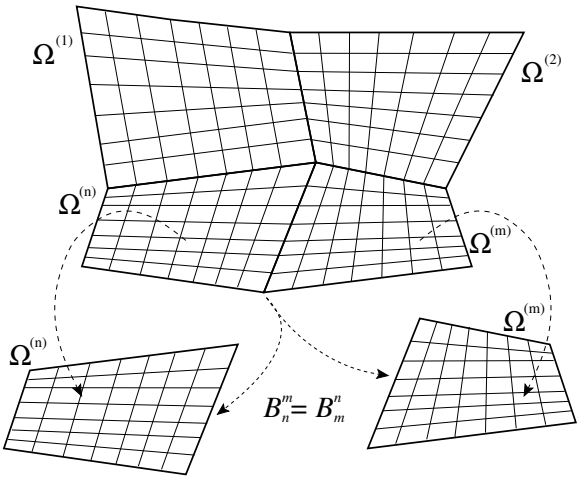

Figure 2: Generic irregular domain configuration and sub-domain decomposition.

used for implementing the connectivity conditions among adjacent elements. Since a generic GDQFEM element can have the edges that are not parallel to the axes of the external Cartesian reference system, the external stresses must be written as functions of the direction cosines of the given boundary as follows

$$\boldsymbol{\sigma}_n = \mathbf{N}\boldsymbol{\sigma}, \quad \text{for} \quad \mathbf{N} = \begin{bmatrix} n_x^2 & n_y^2 & 2n_x n_y \\ -n_x n_y & n_x n_y & n_x^2 - n_y^2 \end{bmatrix} \tag{5}$$

In Eq. 5 the components of the normal vector $\mathbf{n}$ are indicated as n_x and n_y and $\boldsymbol{\sigma}_n = \begin{bmatrix} \sigma_n & \tau_{ns} \end{bmatrix}^T$ is the transformed stress vector from the external Cartesian reference system xyz to the local one nsz, that is depicted in Fig. 1.

3 Generalized differential quadrature finite element method

As it has been stated in the introduction, the GDQFEM decomposes a domain Ω into several sub-domains $\Omega^{(n)}$, for $n = 1, \ldots, n_e$, where n_e is the total number of sub-domains. It is important noticing that a mesh generation in the presence of mechanical irregularities involves element matching and irregular geometries. For the present case every element boundary is exposed to its adjacent elements and two elements are disjoint, that is $\Omega^{(n)} \cap \Omega^{(m)} = \emptyset$, for $n \neq m$. Furthermore, in set-theoretic notation the global domain is given as the union of a collection of sets $\Omega = \Omega^{(1)} \cup \cdots \cup \Omega^{(n_e)}$. In general, the decomposition procedure of GDQFEM follows the general guidelines of FEM. In fact, on every sub-domain the physical parameters must be constants (or, at least, continuous).

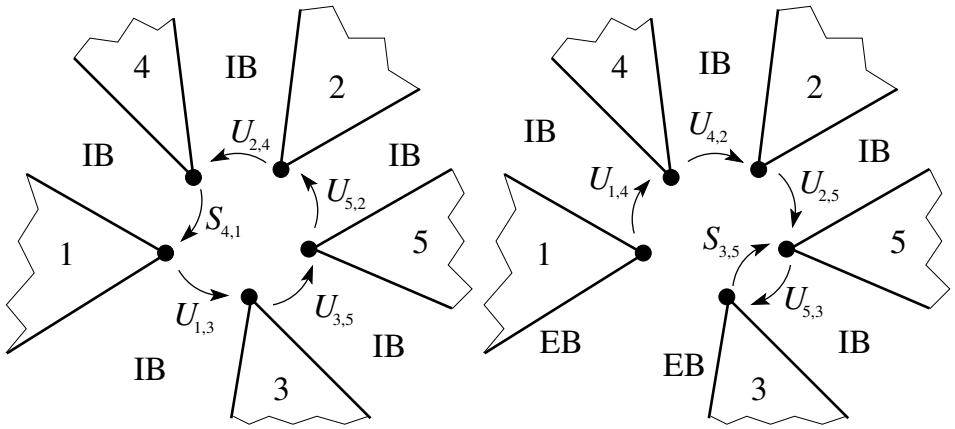

Figure 3: Corner type boundary conditions: a) corner with uniform internal conditions; b) corner under internal and external conditions.

The proposed numerical procedure solves the strong form of the differential problem. Therefore, the fundamental equation Eq. 4 is discretized directly. In general, to approximate the physical problem correctly, distorted elements have to be used in the division procedure. Thus, a coordinate transformation technique must be introduced, in order to map an arbitrarily shaped element from Cartesian coordinates x-y to a parent element in computational coordinates ξ-η as

$$\mathbf{x} = \mathbf{x}(\boldsymbol{\xi}), \text{ for } x = \begin{bmatrix} x & y \end{bmatrix}^T \text{ and } \boldsymbol{\xi} = \begin{bmatrix} \xi & \eta \end{bmatrix}^T \tag{6}$$

Developing the well-known mathematical calculations for coordinate transformation, that can be found in a number of works [Cen, Chen, Li, and Fu (2009); Liu (1999); Xing and Liu (2009); Xing, Liu, and Liu (2010); Zhong and He (1998); Zhong and Yu (2009)], the first Cartesian derivatives are

$$\frac{\partial}{\partial \mathbf{x}} = \frac{1}{\det \mathbf{J}} \begin{bmatrix} \frac{\partial y}{\partial \eta} & -\frac{\partial y}{\partial \xi} \\ -\frac{\partial x}{\partial \eta} & \frac{\partial x}{\partial \xi} \end{bmatrix} \frac{\partial}{\partial \boldsymbol{\xi}} \tag{7}$$

where $\det \mathbf{J} = \frac{\partial x}{\partial \xi}\frac{\partial y}{\partial \eta} - \frac{\partial x}{\partial \eta}\frac{\partial y}{\partial \xi}$. Moreover the second order Cartesian derivatives are

$$\boldsymbol{\partial}^2_{\mathbf{x}} = \boldsymbol{\Xi}^{(2)}_{\mathbf{x}} \boldsymbol{\partial}^2_{\boldsymbol{\xi}} \tag{8}$$

where

$$\begin{aligned}\boldsymbol{\partial}_{\mathbf{x}}^{2} &= \begin{bmatrix} \frac{\partial^2}{\partial x^2} & \frac{\partial^2}{\partial y^2} & \frac{\partial^2}{\partial x \partial y} \end{bmatrix}^T \\ \boldsymbol{\partial}_{\boldsymbol{\xi}}^{2} &= \begin{bmatrix} \frac{\partial}{\partial \xi} & \frac{\partial}{\partial \eta} & \frac{\partial^2}{\partial \xi^2} & \frac{\partial^2}{\partial \eta^2} & \frac{\partial^2}{\partial \xi \partial \eta} \end{bmatrix}^T \end{aligned} \tag{9}$$

and $\boldsymbol{\Xi}_{\mathbf{x}}^{(2)}$ is a differential operator

$$\boldsymbol{\Xi}_{\mathbf{x}}^{(2)} = \begin{bmatrix} \frac{\partial^2 \xi}{\partial x^2} & \frac{\partial^2 \eta}{\partial x^2} & \left(\frac{\partial \xi}{\partial x}\right)^2 & \left(\frac{\partial \eta}{\partial x}\right)^2 & 2\frac{\partial \xi}{\partial x}\frac{\partial \eta}{\partial x} \\ \frac{\partial^2 \xi}{\partial y^2} & \frac{\partial^2 \eta}{\partial y^2} & \left(\frac{\partial \xi}{\partial y}\right)^2 & \left(\frac{\partial \eta}{\partial y}\right)^2 & 2\frac{\partial \xi}{\partial y}\frac{\partial \eta}{\partial y} \\ \frac{\partial^2 \xi}{\partial x \partial y} & \frac{\partial^2 \eta}{\partial x \partial y} & \frac{\partial \xi}{\partial x}\frac{\partial \xi}{\partial y} & \frac{\partial \eta}{\partial x}\frac{\partial \eta}{\partial y} & \frac{\partial \xi}{\partial x}\frac{\partial \eta}{\partial y} + \frac{\partial \xi}{\partial y}\frac{\partial \eta}{\partial x} \end{bmatrix} \tag{10}$$

The general interface of two elements is given by the superposition of the boundary points of the element $\Omega^{(n)}$ and its adjacent element $\Omega^{(m)}$, as depicted in Fig. 2. The external boundary conditions, indicated by B_n^0 are treated as in the classic GDQ method [Tornabene, Viola, and Inman (2009); Viola, Rossetti, and Fantuzzi (2012)], whereas B_n^m and B_m^n must be considered separately. In fact, they denote the continuity conditions of the boundaries of the elements $\Omega^{(n)}$ and $\Omega^{(m)}$. It is worth noticing that compatibility conditions are associated to the governing equations under consideration [Zong, Lam, and Zhang (2005); Fantuzzi (2013)]. In general, continuity conditions can be written as

$$\mathbf{u}^{(n)} = \mathbf{u}^{(m)}, \qquad \boldsymbol{\sigma}_n^{(n)} = \boldsymbol{\sigma}_n^{(m)} \tag{11}$$

where n, m are two adjacent elements. For the sake of clarity the continuity conditions between two facing edges are reported in the following. As far as the kinematic conditions are concerned

$$\begin{bmatrix} u \\ v \end{bmatrix}^{(n)} = \begin{bmatrix} u \\ v \end{bmatrix}^{(m)} \tag{12}$$

where u and v are the displacement parameters of the model of the two facing elements. Since no derivative is involved in Eq. 12, the relations can be written at the discrete nodes of the edges directly. On the contrary, the static conditions are

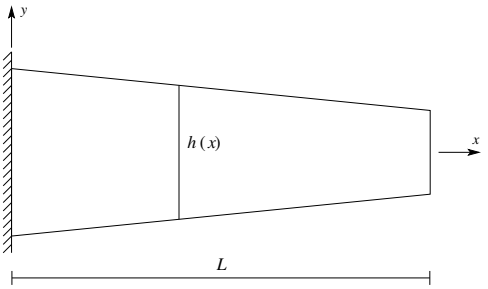

Figure 4: Geometry configuration of a tapered cantilever beam.

Table 1: Eigenvalues of a variable cross-section cantilever elastic beam.

ω [rad/s]	MLPG†	FEM†	$n_e = 1$ $N = 13$	$n_e = 1$ $N = 21$	$n_e = 1$ $N = 31$	$n_e = 1$ $N = 41$
1	263.21	262.09	261.8031	261.6137	261.5746	261.5648
2	293.03	918.93	917.4574	917.5720	917.5941	917.5994
3	953.45	951.86	951.9089	951.9198	951.9247	951.9265
4	1855.14	1850.92	1852.2551	1852.2071	1852.1880	1852.1838
5	2589.78	2578.63	2584.4408	2584.3861	2584.3747	2584.3716
6	-	-	2736.5644	2736.5885	2736.5902	2736.5905
7	-	-	3286.4464	3286.4786	3286.4916	3286.4953
8	-	-	3701.2990	3701.8364	3701.8417	3701.8412
9	-	-	3853.8719	3853.9282	3853.9316	3853.9321
10	-	-	4155.5147	4155.4625	4155.4595	4155.4590

† [Gu and Liu (2001)]

given by the development of Eq. 5.

$$\begin{aligned}
\sigma_n &= \left(\left((2G+\lambda) n_x^2 + \lambda n_y^2 \right) \frac{\partial}{\partial x} + 2G n_x n_y \frac{\partial}{\partial y} \right) u + \\
&+ \left(2G n_x n_y \frac{\partial}{\partial x} + \left((2G+\lambda) n_y^2 + \lambda n_x^2 \right) \frac{\partial}{\partial y} \right) v \\
\tau_{ns} &= \left(-2G n_x n_y \frac{\partial}{\partial x} + G \left(n_x^2 - n_y^2 \right) \frac{\partial}{\partial y} \right) u + \\
&+ \left(G \left(n_x^2 - n_y^2 \right) \frac{\partial}{\partial x} + 2G n_x n_y \frac{\partial}{\partial y} \right) v
\end{aligned} \tag{13}$$

Once the stresses of Eq. 13 are written as functions of the displacement parameters, the GDQ rule can be applied as in [Viola and Tornabene (2005, 2006, 2009)] and the

discretized form of Eq. 13 can be evaluated. It is pointed out that the derivatives of Eq. 13 are written with respect to the external Cartesian system, nevertheless they must be transformed into the computational ξ-η system when the elements are distorted, using coordinate transformation of Eqs. 6,8. Then the static equations can be written as

$$\begin{bmatrix} \sigma_n \\ \tau_{ns} \end{bmatrix}^{(n)} = \begin{bmatrix} \sigma_n \\ \tau_{ns} \end{bmatrix}^{(m)} \tag{14}$$

Since plane elastic problems are considered in the following, the static compatibility conditions are also taken by Eq. 5. Besides, these displacements are set equal at the element interface. It is clear that the numerical conditions across each boundary is of $\mathscr{C}^1$ continuity type, due to the first order derivatives of Eqs. 5,11. The stress components along a generic interface depend on the direction cosines of the outward unit normal vector $\mathbf{n}$, as it appears in Eq. 5. It is pointed out that this kind of boundary conditions has been introduced in the study of revolution shells and toroid in the works [Tornabene, Viola, and Fantuzzi (2013); Tornabene, Fantuzzi, Viola, and Ferreira (2013); Tornabene, Fantuzzi, Viola, and Reddy (2014)], where the same implementation can be followed. In fact, in order to consider a closed domain two edges must be superimposed as in GDQFEM approach. In addition to the element edge conditions, the corner type boundary conditions must be considered. A schematic representation of a generic corner is presented in Fig. 3, where in Fig. 3a) an internal corner is depicted, whereas in Fig. 3b) a corner that connects internal and external boundaries is shown. The symbol EB denotes the external boundaries and IB indicates the internal boundaries. As shown by the corners configurations in Fig. 3 more than two compatibility conditions have to be enforced. Therefore, at the same time, it is not possible to impose a static and a kinematic boundary condition on the current points as in Eqs. 12,14. Hence, with reference to Fig. 3a), kinematic conditions are enforced at the adjacent elements. It is noted that $U_{n,m} \rightarrow U^{(n)} = U^{(m)}$ indicates the generic displacement parameter u or v. Thus, these kinematic conditions lead to

$$\begin{cases} U^{(1)} = U^{(3)} \\ U^{(3)} = U^{(5)} \\ U^{(5)} = U^{(2)} \\ U^{(2)} = U^{(4)} \end{cases} \Rightarrow U^{(4)} = U^{(1)} \tag{15}$$

Since several static conditions can be imposed, the implementation choice was to set the parameters equality of the two facing elements, such $S_{4,1} \rightarrow S^{(4)} = S^{(1)}$, where $S_{4,1}$ represents one of the two stresses σ_n and τ_{ns} that are written as functions of the displacement parameters and the direction cosines of the current facing

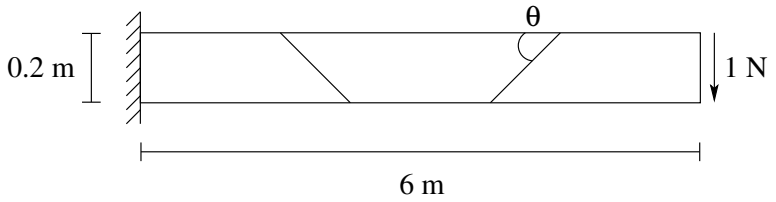

Figure 5: MacNeal's beam three elements mesh under shear force.

Table 2: Normalized tip deflection of MacNeal's thin beam for different mesh geometries.

Exact†	1.000 (0.1081 m)		
FEM‡	Regular 0.993	Parallelogram 0.985	Trapezoidal 0.988
GDQFEM	$n_e = 1$ 0.99882	$n_e = 3, \theta \approx \pi/6$ 0.99775	$n_e = 3, \theta \approx \pi/18$ 1.00031

† [Cen, Chen, Li, and Fu (2009)], ‡ [Rezaiee-Pajand and Karkon (2013)]

normal **n**. In a similar manner, when a free boundary condition in Fig. 3b) is imposed externally (EB = free), the last static condition cannot be enforced across the two external conditions, because it gives rise to numerical instabilities. So, the algorithm imposes it between the last two elements, that is $S_{3,5} \rightarrow S^{(3)} = S^{(5)}$. It is pointed out that, for the case depicted in Fig. 3b), if one of the external boundaries is clamped, all of these conditions do not have to be applied, because the corner is fixed, so five clamped conditions are imposed. For a complete survey of the corner and edge boundary conditions, the interested reader can refer to the work [Viola, Tornabene, and Fantuzzi (2013b)].

4 Worked out examples

The GDQFEM is used in the study of static and dynamic behaviour of two dimensional structures. For all the computations, a Chebyshev-Gauss-Lobatto (C-G-L) grid distribution is used. The aforementioned grid has widely been known in literature for carrying out the most accurate results based on GDQ method [Marzani, Tornabene, and Viola (2008); Ferreira, Viola, Tornabene, Fantuzzi, and Zenkour (2013); Tornabene, Fantuzzi, Viola, Cinefra, Carrera, Ferreira, and Zenkour (2014)]. Since a 2D GDQ problem is solved, two grid point numbers must be chosen. The

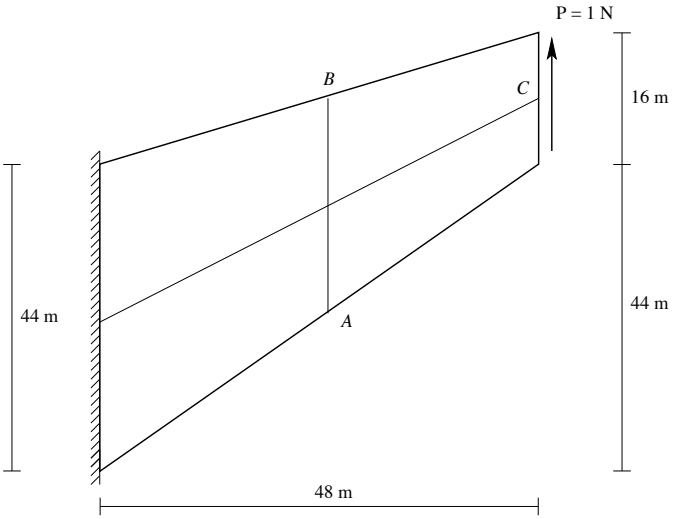

Figure 6: Cook's cantilever beam geometry.

C-G-L points are located as

$$\begin{aligned} \xi_i &= -\cos\left(\frac{i-1}{N-1}\pi\right), \text{ for } i = 1,\ldots,N \\ \eta_j &= -\cos\left(\frac{j-1}{M-1}\pi\right), \text{ for } j = 1,\ldots,M \end{aligned} \tag{16}$$

where ξ and η are the parent element coordinates due to mapping transformation and $\xi,\eta \in [-1,1]$. When the same number of grid points is considered along the two main element directions, N indicates the number of grid points along each of the two directions themselves. The first example analyzes the free vibrations of a cantilever beam with variable cross-section. The beam geometry is depicted in Fig. 4. It is mentioned that the present case has been taken from the work by [Gu and Liu (2001)], where a Meshless Local Petrov-Galerkin (MLPG) method is developed and used for solving several dynamic 2D problems. The beam has a length of $L =$ 10 m and the tapered height is defined by $h(x=0) = 5$ m, $h(x=L) = 3$ m. As far as the mechanical properties are concerned the material is elastic, homogeneous and isotropic, with Young's modulus $E = 3\cdot 10^7$ Pa, Poisson's ratio $\nu = 0.3$ and density $\rho = 1$ kg/m^3. The current problem has been solved using a single distorted element for several numbers of grid points. The convergence of the results is reported in Tab. 1, where the present solution is compared with a FEM solution and the MLPG solution obtained by [Gu and Liu (2001)]. In order to assess the capabilities of

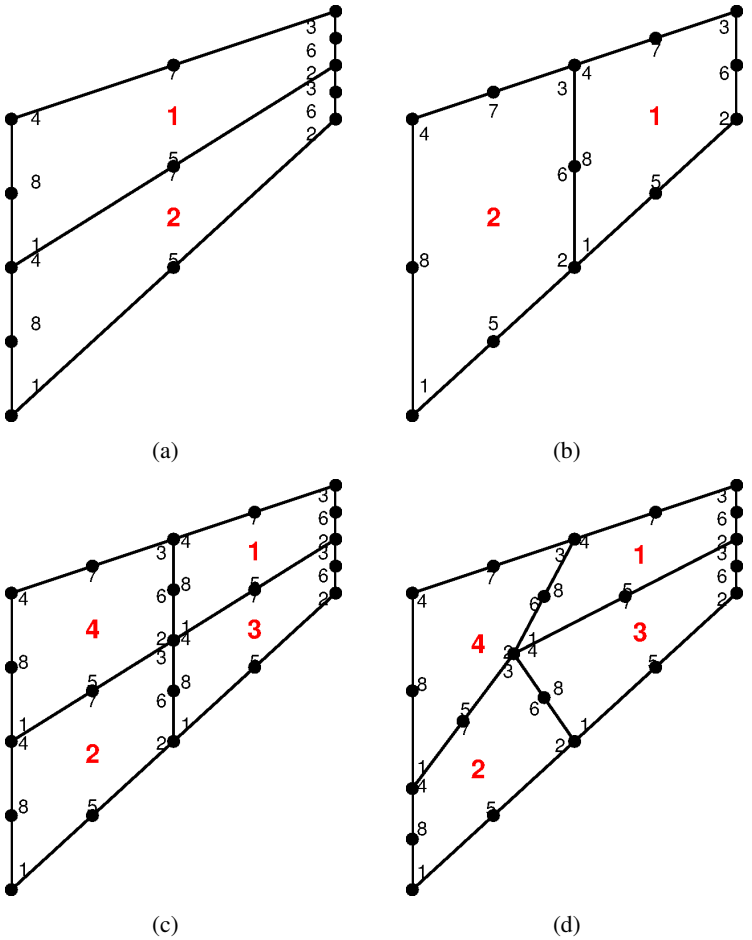

Figure 7: Cook's beam GDQFEM meshes: a) two element mesh after horizontal division; b) two element mesh after vertical division; c) four element mesh within a regular division; d) four element distorted mesh.

the suggested methodology, some other classic FEM benchmarks are proposed. In the following, the MacNeal's beam is analysed. For the sake of conciseness, a three elements mesh is considered in the present paper, nevertheless a complete study of the FEM MacNeal's beam can be found in [Macneal and Harder (1985); Rezaiee-Pajand and Karkon (2013)]. In fact, this investigation has become a classic benchmark for measuring accuracy and testing the sensitivity to mesh distortion for 2D elastic plane elements. For the present case, the beam length is $L = 6$ m and the height is $H = 0.2$ m. The model has a constant thickness $h = 0.1$ m, so a plane

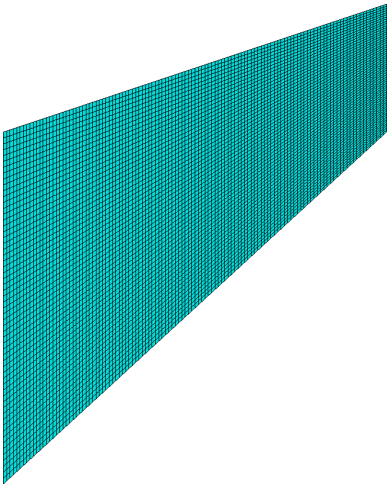

Figure 8: Cook's cantilever beam FEM mesh of $n_e = 6960$ S8R type (Abaqus) elements.

stress case is considered. The MacNeal's beam elastic modulus is $E = 10$ MPa and Poisson's ratio is $\nu = 0.3$. The external applied load is a shear force $F = 1$ N, distributed along the element edges, and a static problem is solved. The results in terms of tip's deflection of the thin beam are reported in Tab. 2, where the GDQFEM results are put at the bottom of the list arranged in rows and including the exact solution by [Cen, Chen, Li, and Fu (2009)] and a FEM solution from [Rezaiee-Pajand and Karkon (2013)]. The numerical results reported in Tab. 2 are dimensionless with respect to the exact solution [Cen, Chen, Li, and Fu (2009)]. In fact, on the first line the tip displacement is equal to 0.1081 m that is considered congruent to 1. On the second line, the numerical FEM solution by [Rezaiee-Pajand and Karkon (2013)] is reported for three kinds of mesh. The GDQFEM solution is calculated for trapezoidal mesh only, where the slope θ indicates the angle between the inclined edge and the horizontal edge. It is noted that, for a highly distorted mesh with $\theta = \pi/18 = 10^\circ$, the numerical solution is still in good accordance with the exact solution, whereas the numerical results by [Rezaiee-Pajand and Karkon (2013)] were obtained with $\theta = \pi/8 = 22.5^\circ$. Since in the previous example a regular geometry has been considered, an irregular and very common geometry is studied in the following. A very popular benchmark, which has been used for testing the sensitivity and efficiency of any FEM, is the Cook's cantilever beam [Cook (2001)]. The structure geometry is depicted in Fig. 6, where the cantilever dimensions and loads are reported. The solutions in terms of displacements and stresses are calculated at three points A, B and C and reported in Tab. 3. The

Table 3: Numerical comparison for the Cook's beam.

	FEM	Ref. †	Ref. ‡	GDQFEM $n_e = 1$		
				$N = 21$	$N = 35$	$N = 41$
				$M = 21$	$M = 27$	$M = 31$
$\sigma_{A,max}$	0.2369	0.2362	0.2367	0.2374	0.2371	0.2367
$\sigma_{B,min}$	-0.2035	-0.2023	-0.2039	-0.2034	-0.2060	-0.2014
$u_{y,C}$	23.961	23.96	23.90	24.0627	23.9690	23.9677
	GDQFEM $n_e = 2$ (vertical)			GDQFEM $n_e = 2$ (horizontal)		
	$N = 21$	$N = 31$	$N = 41$	$N = 21$	$N = 31$	$N = 41$
	$M = 21$	$M = 31$	$M = 31$	$M = 11$	$M = 21$	$M = 21$
$\sigma_{A,max}$	0.2379	0.2374	0.2383	0.2367	0.2371	0.2369
$\sigma_{B,min}$	-0.1970	-0.1992	-0.1943	-0.1967	-0.2050	-0.2009
$u_{y,C}$	23.9790	23.9717	23.9665	23.9644	23.9973	23.9680
	GDQFEM $n_e = 4$ (regular)			GDQFEM $n_e = 4$ (distorted)		
	$N = 21$	$N = 23$	$N = 31$	$N = 21$	$N = 23$	$N = 31$
	$M = 21$	$M = 17$	$M = 21$	$M = 21$	$M = 17$	$M = 21$
$\sigma_{A,max}$	0.2371	0.2369	0.2369	0.2366	0.2368	0.2369
$\sigma_{B,min}$	-0.2032	-0.1982	-0.1980	-0.1962	-0.1773	-0.1726
$u_{y,C}$	24.0021	23.9756	23.9691	23.9431	23.9196	23.9386

† [Yuqiu and Yin (1994)], ‡ [Rezaiee-Pajand and Karkon (2013)]

beam is subjected to a constant shear force load $P = 1$ N, distributed along the free edge and the beam is assumed to be linearly elastic, homogeneous and isotropic, within $E = 1$ Pa and $\nu = 1/3$. It should be emphasized that four different meshes have been studied. They are all graphically reported in Fig. 7, where two of them are made of two elements and each of the other two consists of four elements. In particular, the mesh in Fig. 7d) is a specially distorted mesh. Furthermore, the FEM mesh used in the numerical comparison is reported in Fig. 8. In particular it is composed of $n_e = 6960$ elements with eight nodes. The GDQFEM results are compared with the solutions found by [Yuqiu and Yin (1994); Rezaiee-Pajand and Karkon (2013)] and a FEM solution obtained by using commercial code. Very good agreement is observed for all the computations, both in terms of displacements and stresses. It is underlined that sometimes the grid point numbers are not equal along the two element edges. In fact, it is sufficient that all the adjacent edges have the same number of points in order to have a compatible connectivity.

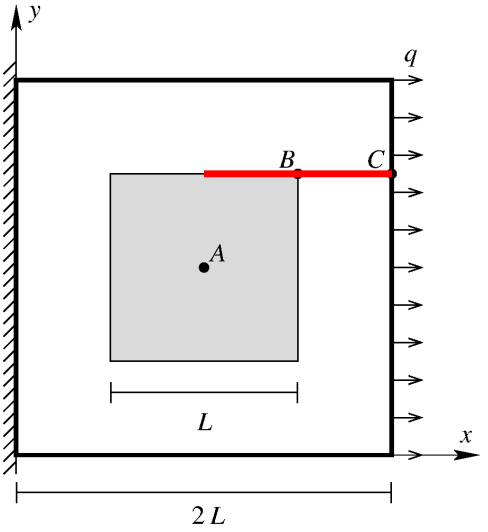

Figure 9: Geometry of a square plate with a square inclusion under uniform tension.

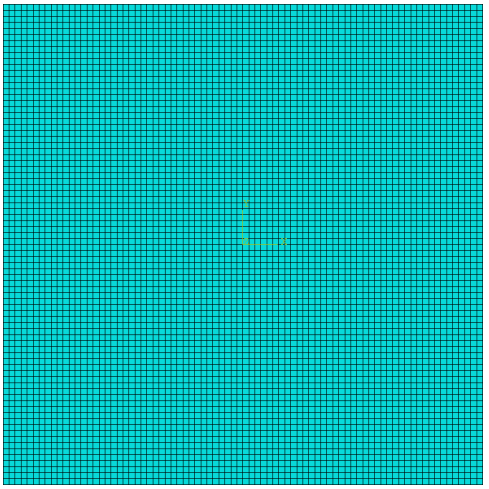

Figure 10: FEM mesh of a square plate with a square inclusion with $n_e = 6400$ S8R type (Abaqus) elements.

In the second part of the numerical applications proposed in this paper, some simulations about material discontinuities will be proposed. As mentioned before, a discontinuity along a material interface is implemented as a compatibility condition between adjacent elements. In particular, for the current methodology kinematic

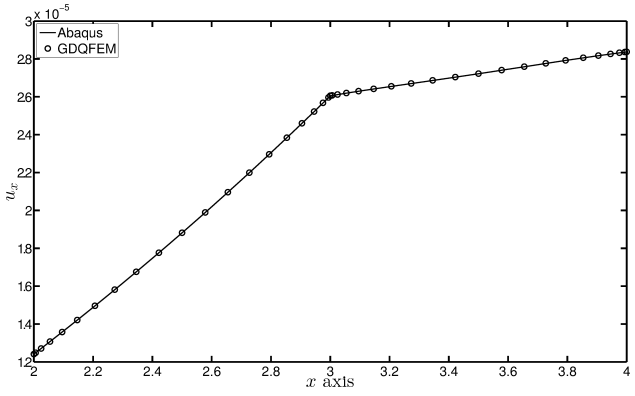

(a)

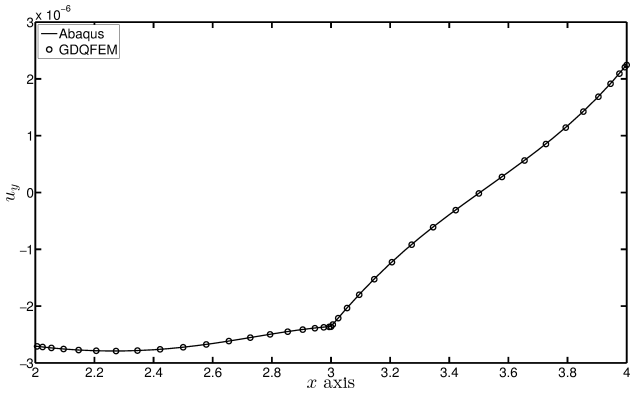

(b)

Figure 11: Square plate with a square inclusion: a) horizontal displacement $u = u_x$; b) vertical displacement $v = u_y$.

and static compatibility conditions are imposed. So, the continuity between two elements is $\mathscr{C}^1$ type, whereas in some FEM applications the standard compatibility is generally $\mathscr{C}^0$. In the first example, of the second part of the numerical results, a square plate with a square inclusion under a uniform tension and clamped along one side is considered. In Fig. 9, the plate geometry is presented with the external applied load. The present case is reported in the book by [Zong and Zhang (2009)]. The plate side is $2L = 4$ m and the external load $q = 100$ N/m. The matrix material has $E_1 = 3 \cdot 10^7$ N/m^2, $\nu_1 = 0.3$, whereas the inclusion has $E_2 = 3 \cdot 10^6$ N/m^2, $\nu_2 = 0.25$. Fig. 10 represents the FEM mesh used in the computation and from which the following plots are obtained. The FEM model is made of $n_e = 6400$ elements with eight nodes. The red solid line, indicated in Fig. 9, refers to the

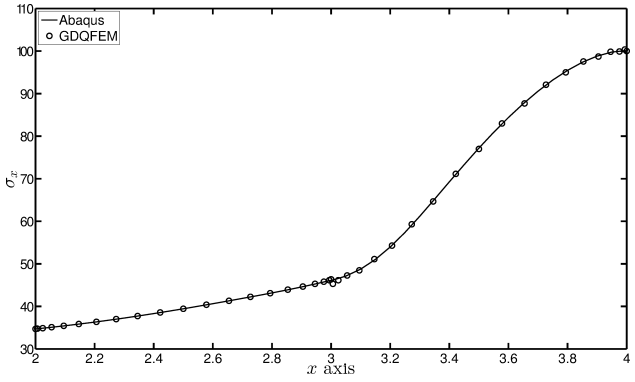

(a)

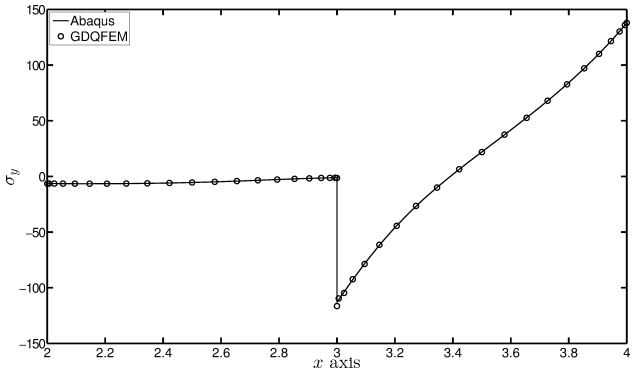

(b)

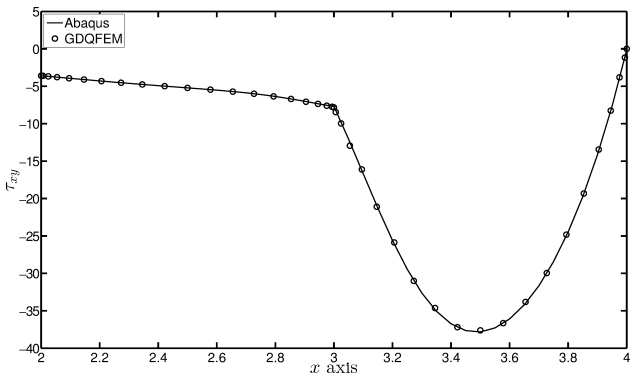

(c)

Figure 12: Square plate with a square inclusion: a) normal stress σ_x; b) normal stress σ_y; c) shear stress τ_{xy}.

Table 4: Convergence of the GDQFEM results for the square plate with a square inclusion

N	σ_{xA}	σ_{yA}	$u_{xB} \cdot 10^6$	$u_{yB} \cdot 10^6$	σ_{xC}
7×7	38.5153	-6.9317	19.7554	-3.6159	100.0000
9×9	38.3985	-7.0648	19.7935	-3.6468	100.0000
11×11	38.3530	-7.1166	19.8141	-3.6722	100.0000
13×13	38.3300	-7.1423	19.8268	-3.6909	100.0000
15×15	38.3166	-7.1572	19.8353	-3.7049	100.0000
21×21	38.2980	-7.1775	19.8492	-3.7303	100.0000
FEM	38.2677	-7.2084	19.8945	-3.74357	99.8991

Table 5: Results of a square plate with a circular inclusion

N	σ_{xA}	σ_{yA}	$u_{yB} \cdot 10^6$	σ_{yB}
7×7	-6.6406	33.3275	32.1107	100.0000
9×9	-6.5731	33.2575	32.0298	100.0000
11×11	-6.5719	33.2453	32.0189	100.0000
13×13	-6.5746	33.2422	32.0174	100.0000
15×15	-6.5771	33.2411	32.0174	100.0000
21×21	-6.5813	33.2403	32.0181	100.0000
FEM	-6.5856	33.2365	32.0232	99.6211

plotting intervals of Figs. 11,12, where displacements and stresses are represented, respectively. In particular, the GDQFEM solution, depicted with black circles, is compared to a FEM solution, drawn with a solid black line. A 21×21 C-G-L grid point distribution is considered in the computation and very good agreement is observed with the reference FEM solution for both displacements and stresses profiles. It is worth noticing that, due to material discontinuity, there is a finite stress jump in Fig. 12b) and a sharp turning point in Fig. 12c). Fig. 9 shows three points indicated by A, B and C, where displacements and stresses are computed in order to have a punctual comparison with FEM, as reported in Tab. 4. The numerical convergence illustrated by Tab. 4 shows stable and accurate results for all the presented numerical grids. It is also noticed that, due to the used higher-order scheme, the stress recovered at the point C is equal to the external applied load, whereas FEM gives an approximation of this value.

In the second example, a square plate with a circular inclusion is considered [Zong and Zhang (2009)]. The plate side is $L = 5$ m and the external load is $q = 100$ N/m. The matrix and inclusion materials are taken from the previous case, such

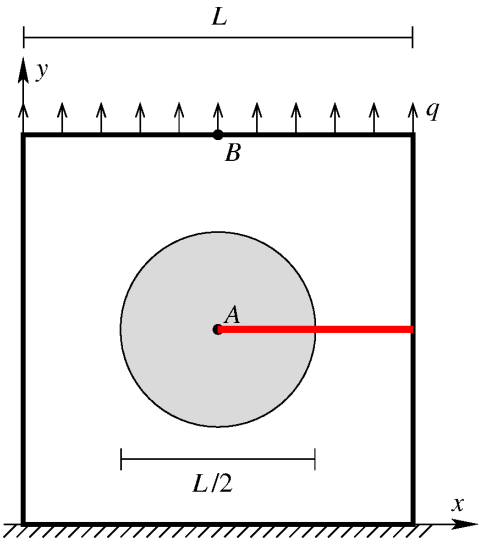

Figure 13: Geometry of a square plate with a circular inclusion.

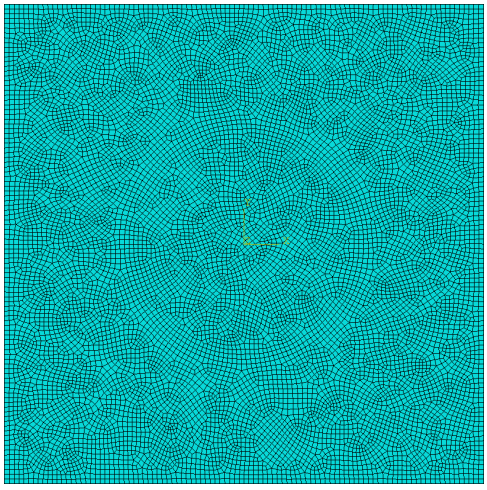

Figure 14: FEM mesh of a square plate with a circular inclusion with $n_e = 12224$ and S8R type (Abaqus) elements.

as $E_1 = 3 \cdot 10^7$ N/m^2, $\nu_1 = 0.3$ and $E_2 = 3 \cdot 10^6$ N/m^2, $\nu_2 = 0.25$. In this case, mapping technique must be used because of the circular boundaries of the inner inclusion. In the computation 8-node elements have been considered. In order to map the circle at least 4 elements must be used, as reported in several examples

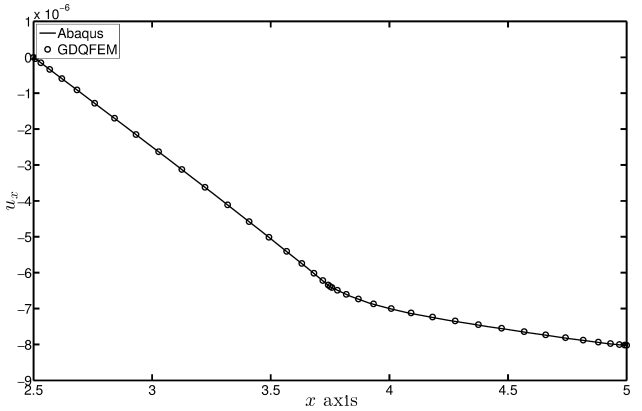

(a)

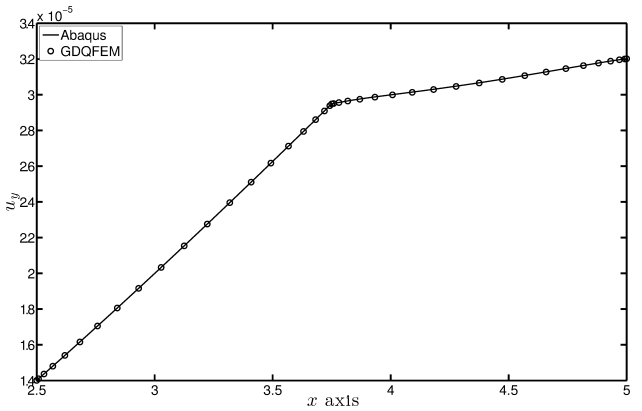

(b)

Figure 15: Square plate with a circular inclusion: a) horizontal displacement $u = u_x$; b) vertical displacement $v = u_y$.

[Fantuzzi (2013)]. So, $n_e = 12$ is considered for the current computation. The FEM mesh is shown in Fig. 14, where $n_e = 12224$ elements with eight nodes. The displacement and stress comparison is performed for the points along the red solid line of Fig. 13 and the punctual displacements and stresses are calculated in A and B of Fig. 13. A distribution of 21×21 grid points distribution is considered for all the plots depicted in Figs. 15,16, where very good agreement is observed between the GDQFEM results and the ones by FEM. The meaning of the symbols is the same as the previous case, so the black solid line represents the FEM solution and the black circles stand for the GDQFEM solution. From Fig. 15 it appears that there is, for both the in-plane displacements, a sharp turning point due to the two

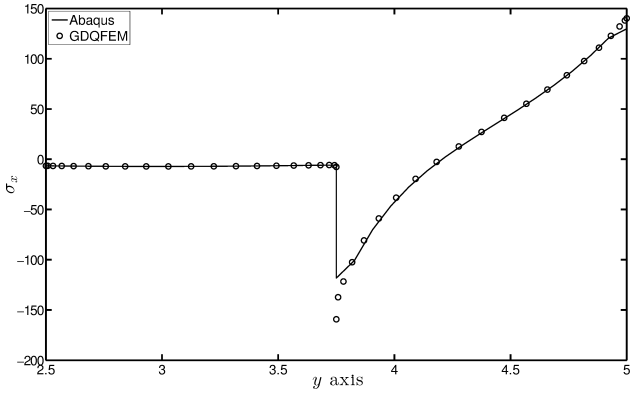

(a)

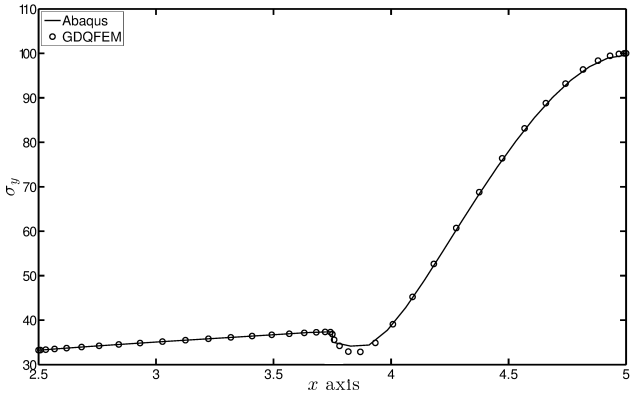

(b)

Figure 16: Square plate with a circular inclusion: a) normal stress σ_x; b) normal stress σ_y.

different derivatives at the material interface. In Fig. 16a) a finite stress jump at the interface between the inclusion and the matrix appears for the horizontal stress σ_x, where as in Fig. 16b) the normal stress σ_y does not show any discontinuity at the interface, but the stress function oscillates when the mechanical properties change. The GDQFEM convergence is summarized in Tab. 5, where displacements and stresses at the two points A and B indicated in Fig. 13 are reported. The recovered stress σ_y at the point B is equal to the applied external load, whereas the FEM model has a value that is near to the applied external force, due to the low-order differentiation scheme. In addition to the previous examples, the following comparison is worked out considering the paper by [Dong and Atluri (2012d)] as a reference. The problem under consideration is the classic study of an infinite

Table 6: Computed horizontal and vertical displacements of the external node K for the problem under consideration.

	Elastic inclusion		Rigid inclusion		Void	
	u_2	v_2	u_2	v_2	u_2	v_2
Exact Solution	0.9986	0.2501	0.9964	0.2502	1.0069	0.2506
VCFEM-TT-BVP	0.9947	0.2480	0.9866	0.2446	1.0268	0.2634
VCFEM-TT-C	0.9947	0.2480	0.9866	0.2446	1.0268	0.2635
VCFEM-HS-PCE	1.0589	0.1855	1.0567	0.1828	2.0713	0.9333
GDQFEM	1.0013	0.2543	1.0036	0.2609	0.9893	0.2268

plate with a circular elastic/rigid inclusion or hole subjected to a remote tension P. The radius of the circular inclusion/hole is indicated by R. A plane stress state is investigated. The material properties of the matrix are $E_m = 1$ Pa, $\nu_m = 0.25$. An elastic inclusion is considered, whose material properties are $E_c = 2$ Pa, $\nu_c = 0.3$. The magnitude of the remote tension $P = 1$ N/m and the radius of the inclusion/void is $R = 0.1$ m. Since it is not possible to implement an infinite plate with element of a finite dimension a truncate plate of sides $L = 2$ m is studied. The choice $L/R = 20$ is based on the results obtained by [Li and Viola (2013)], in dealing with the size effect investigation of a central interface crack contained in both bonded finite and infinitive dissimilar materials. Furthermore, to correctly implement the doubly symmetry condition a quarter of it is modeled. The GDQFEM mesh used in the computations is depicted in Fig. 17. The present GDQFEM solution is compared with the ones already shown in the paper [Dong and Atluri (2012d)]. In particular, Tab. 6 shows the comparison of the in-plane displacements of several methods and GDQFEM. Good agreement is observed among all the theories. The stress σ_x along the y axis and σ_y along the x axis are also computed and compared to the exact solution and other theories. It should be noted that the GDQFEM mesh was not changed among the examples. In fact, for the rigid inclusion an elastic modulus $E_c = 10^6$ Pa and for the void $E_c = 10^{-6}$ Pa is taken into account. It can be seen that good agreement is observed among the curves shown in Figs. 18-20 for all the listed cases: elastic and rigid inclusions as well as a void. It is noted that the GDQFEM results are obtained by using a 35×35 grid for each element of the current mesh (Fig. 17).

In the final example, a cantilever elastic beam with an elastic inclusion is investigated. The sample geometry depicted in Fig. 21 is taken from the work by [Wu, Guo, and Askari (2013)]. The beam is $L = 4$ m long, and $D = 1$ m high. A vertical force $P = 1$ kN/m is distributed along the free right edge of the beam. The reference FEM mesh is depicted in Fig. 22, where $n_e = 12296$ elements with eight nodes are

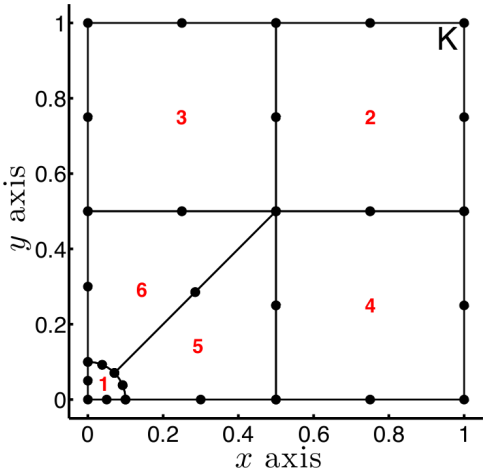

Figure 17: Reference GDQFEM mesh for the comparison with the work by [Dong and Atluri (2012d)].

used. The mechanical properties of the matrix are $E = 2 \cdot 10^7$ Pa, $\nu = 0.3$ and the ones of the circular inclusion are $E = 2 \cdot 10^{10}$ Pa and $\nu = 0.3$. It is noted that the inclusion radius is $R = 0.4$ m, with its center location defined by $L_1 = 2.11$ m and $D_1 = 0.5$ m. The GDQFEM mesh composed of $n_e = 16$ is shown in Fig. 23a). In order to map a circle correctly, four elements are used in the GDQFEM mesh. Fig. 23a) also indicates five cross sections, where GDQFEM displacements and stresses are compared with the ones by FEM and CM in the following. It is interesting to note that, looking at the deformed Von Mises contour plot in Fig. 23b), the colour mapping of the inclusion is different from the matrix due to the different mechanical properties. The through-the-thickness plots concerning displacements and stresses of the current cantilever beam are represented by Figs. 24-26. The GDQFEM solution is compared with the corresponding ones obtained by using FEM and CM. The CM solution is indicated by a blue solid line, the GDQFEM solution is represented by black circles and the FEM results are shown by black crosses. In particular, the horizontal and vertical displacements at $x = 2.11$ m, that is the mid section of the inclusion, are reported in Fig. 24. The normal stress σ_x and the shear stress τ_{xy} are represented in five distinct sections in Figs. 25,26, respectively. The first examined section is located before the inclusion and the second divides the inclusion into two equal parts. The other three sections are put on the right of the inclusion as shown in fig. 23a). Regarding the normal stress σ_x, for the sections located in the matrix material ($x = 3$ m, $x = 3.5$ m) the stress has the classic linear trend as shown in Figs. 25d),e). For the sections just before and after the inclusion ($x = 1.71$

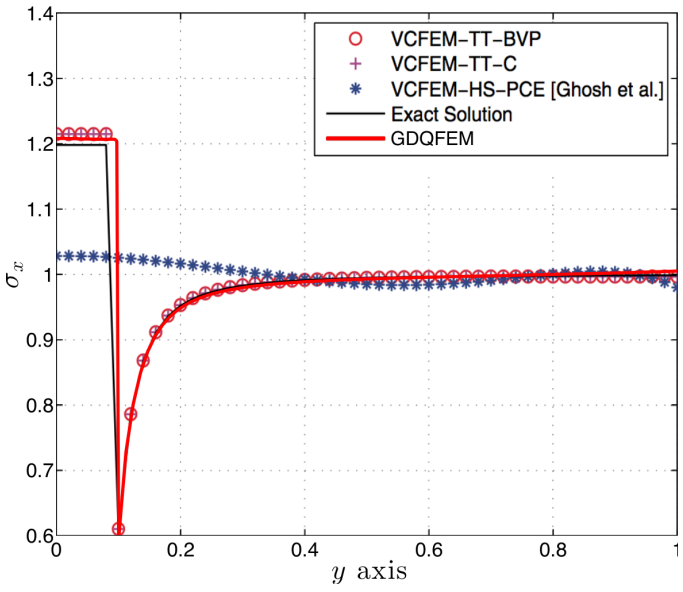

(a)

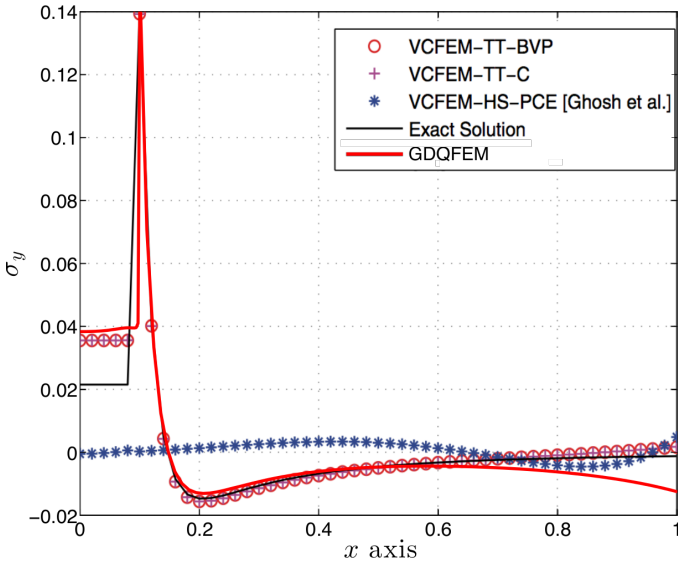

(b)

Figure 18: Normal stresses computed for an infinite plate with an elastic inclusion: a) σ_x along y axis, b) σ_y along x axis.

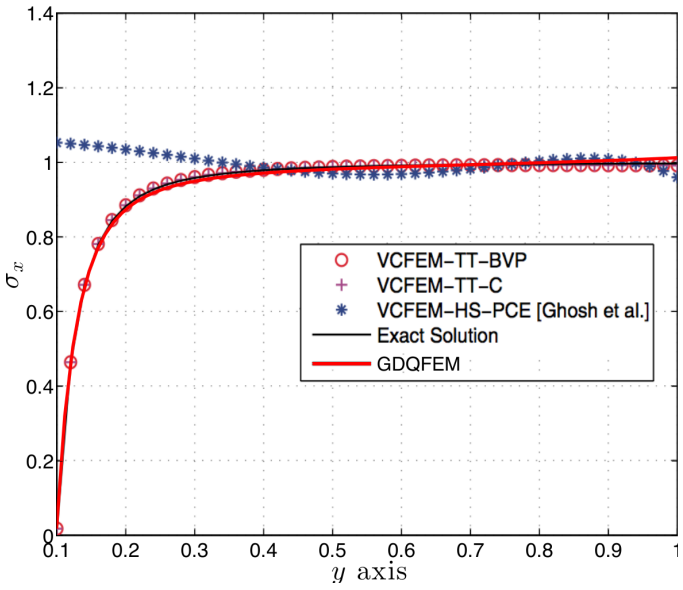

(a)

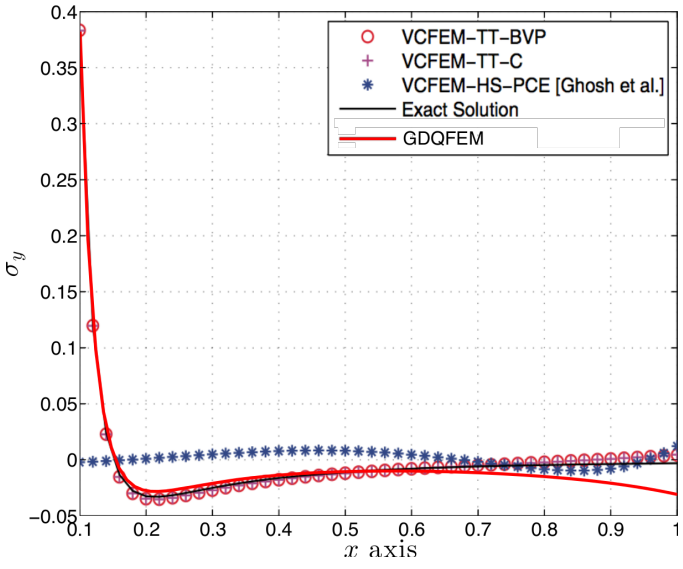

(b)

Figure 19: Normal stresses computed for an infinite plate with a rigid inclusion: a) σ_x along y axis, b) σ_y along x axis.

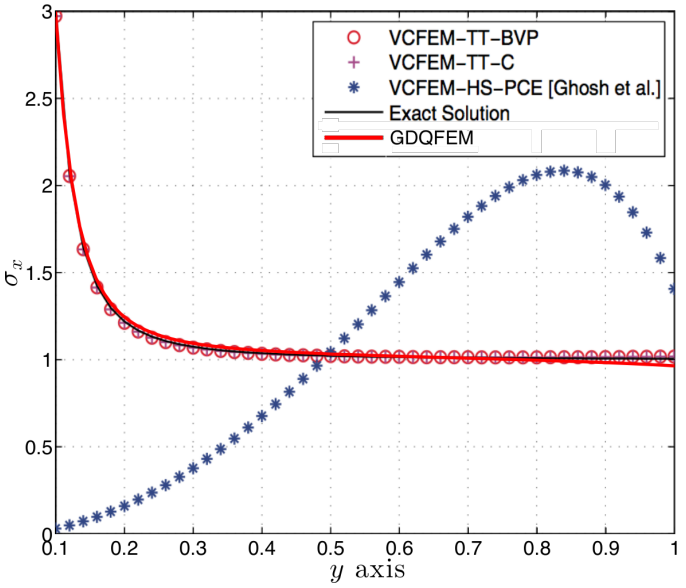

(a)

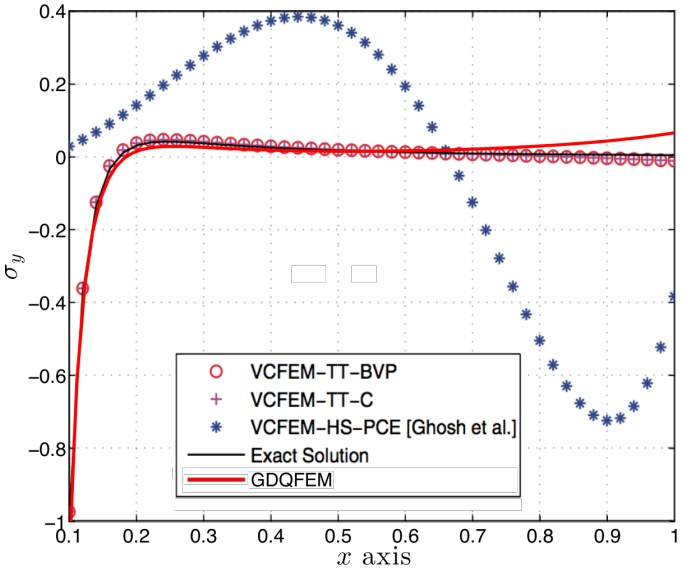

(b)

Figure 20: Normal stresses computed for an infinite plate with a void: a) σ_x along y axis, b) σ_y along x axis.

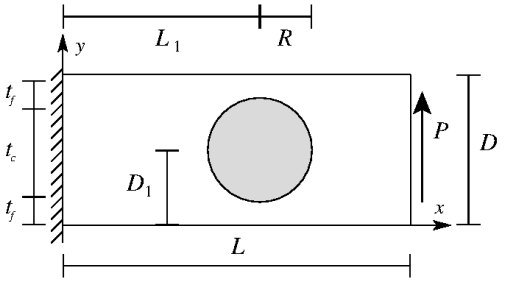

Figure 21: Geometry and loading condition for a cantilever beam.

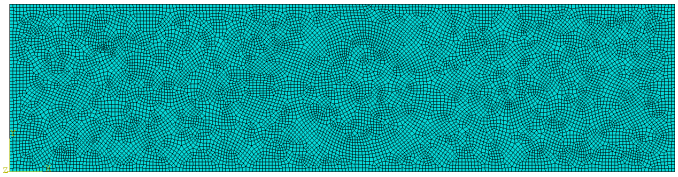

Figure 22: FEM mesh of a composite cantilever beam with $n_e = 12296$ S8R type (Abaqus) elements.

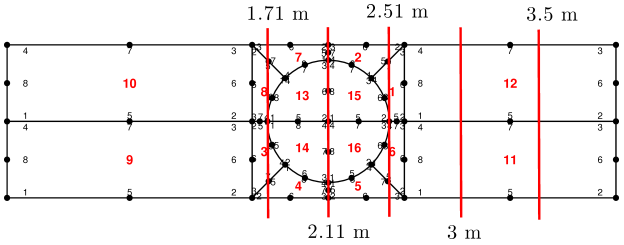

(a)

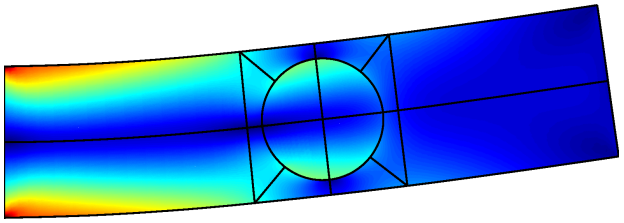

(b)

Figure 23: Cantilever composite beam with an elastic inclusion: a) GDQFEM mesh and five marked cross sections; b) Mises contour plot and deformed shape.

m, $x = 2.51$ m), the stress in Figs. 25a),c) has a nonlinear and continuous trend, because the material is still homogeneous in those parts. Finally, at $x = 2.11$ m the stress is non linear and shows two finite jumps at the material interfaces, due to the different values of the elastic moduli. Analogous comments can be made about the shear stress profiles depicted in Fig. 26. In fact, the classic parabolic trend can be seen in Figs. 26d),e) at $x = 3$ m, $x = 3.5$ m, respectively. The curves do not have a parabolic shape before and after the inclusion. Finally, two different slopes are observed in Fig. 26c) at $x = 2.11$ m.

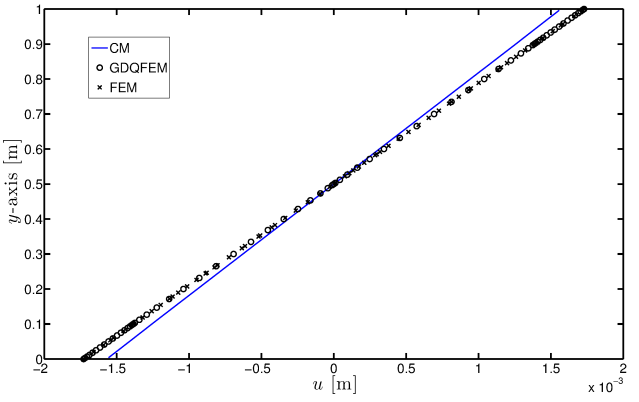

(a)

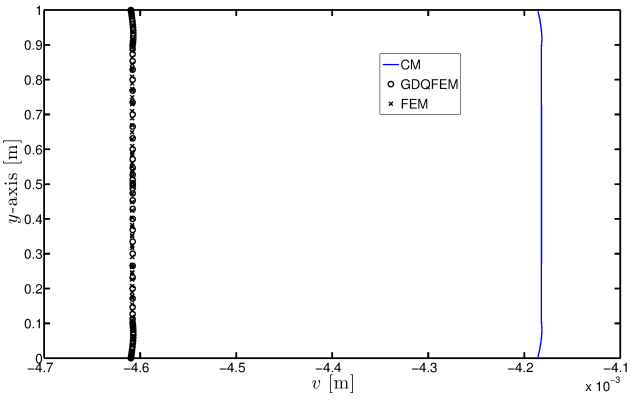

(b)

Figure 24: Displacements at the vertical section $x = 2.11$ m: a) axial displacement u; b) vertical displacement v.

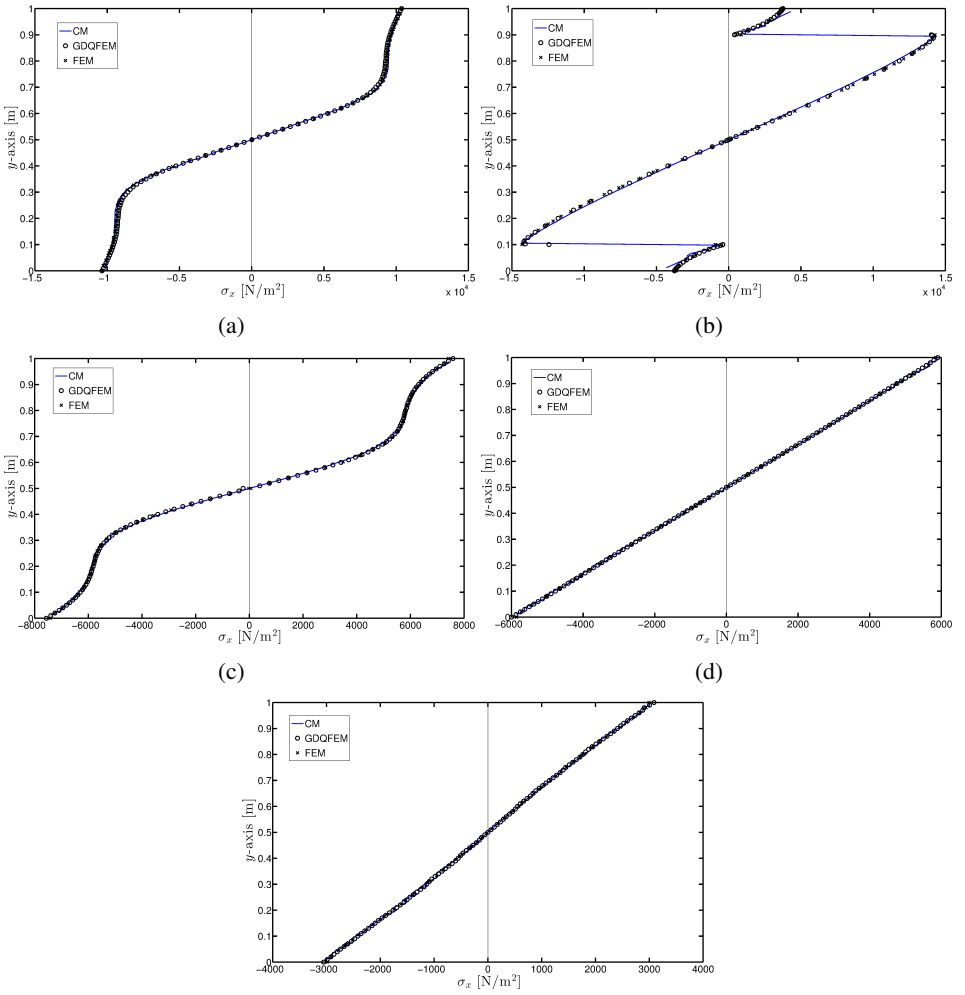

Figure 25: Normal stress σ_x at: a) $x = 1.71$ m; b) $x = 2.11$ m; c) $x = 2.51$ m; d) $x = 3$ m; e) $x = 3.5$ m.

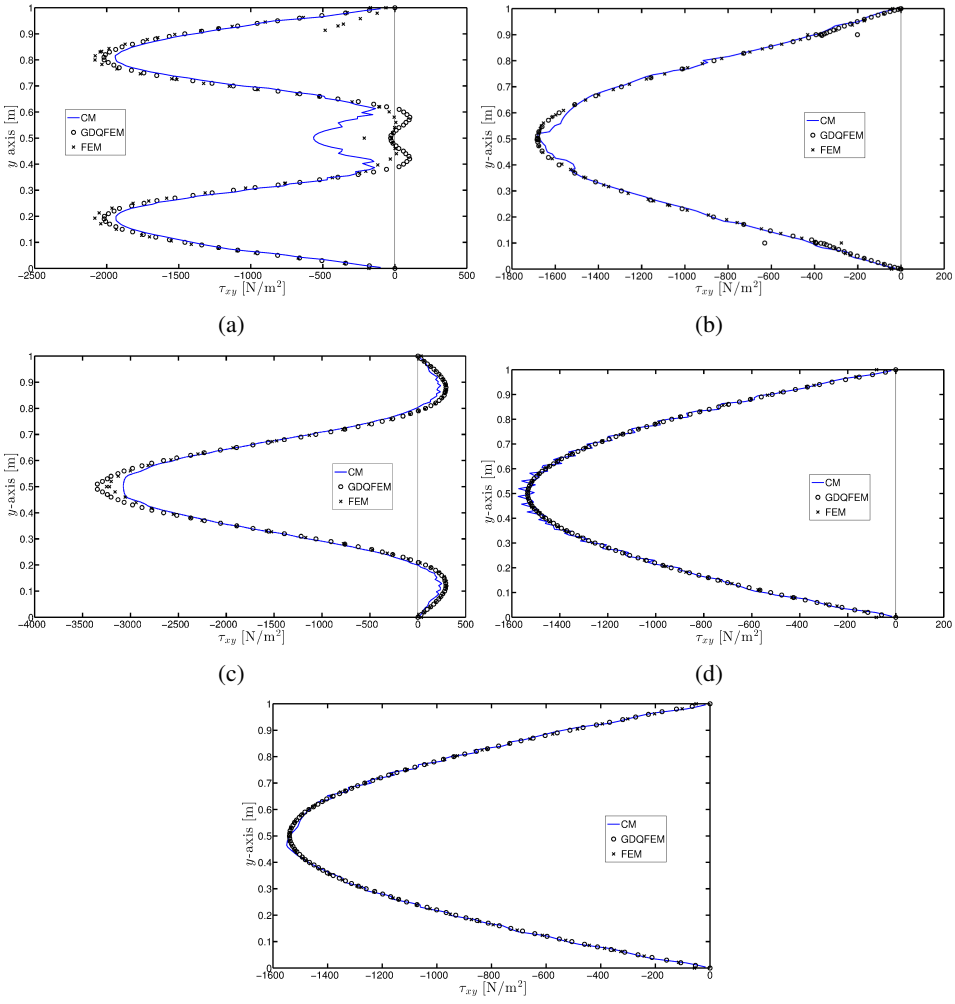

Figure 26: Shear stress τ_{xy} at: a) $x = 1.71$ m; b) $x = 2.11$ m; c) $x = 2.51$ m; d) $x = 3$ m; e) $x = 3.5$ m.

5 Conclusions

In this paper, an advanced version of the classic GDQ method is proposed for solving composite two dimensional linearly elastic problems. This method is based on the strong form of the fundamental system of equations. The problem is formulated on the actual physical displacements. It was observed that GDQFEM leads to very accurate results when compared with FEM and CM. The meshfree quality of GDQ remains at the sub-domain level, whereas the numerical technique is based globally on a predefined mesh that basically divides homogeneous model areas. Therefore, each sub-domain should follow the rules of FEM elements: homogeneous properties and loads. However, since it is possible to increase the approximating polynomial, some GDQFEM elements can be more distorted than the FEM elements. Several two dimensional composite solid examples were provided to examine the effectiveness and the accuracy of the present method. The numerical results indicate that the GDQFEM convergence rate is very fast with respect to the well-known FEM. The interface problem is dealt with a compatibility condition between two adjacent elements. It results in a $\mathscr{C}^1$ condition type, because the equality of displacements and stresses is imposed. This feature simplifies the implementation, because it has been shown that a continuity condition works both for homogeneous and non-homogeneous two dimensional problems.

Acknowledgement: This research was supported by the Italian Ministry for University and Scientific, Technological Research MIUR (40 % and 60 %). The research topic is one of the subjects of the Centre of Study and Research for the Identification of Materials and Structures (CIMEST)-"M. Capurso" of the University of Bologna (Italy).

References

Artioli, E.; Gould, P. L.; Viola, E. (2005): A differential quadrature method solution for shear-deformable shells of revolution. *Engineering Structures*, vol. 27, no. 13, pp. 1879–1892.

Bert, C. W.; Malik, M. (1996): The differential quadrature method for irregular domains and application to plate vibration. *International Journal of Mechanical Sciences*, vol. 38, no. 6, pp. 589–606.

Cen, S.; Chen, X.-M.; Li, C. F.; Fu, X.-R. (2009): Quadrilateral membrane elements with analytical element stiffness matrices formulated by the new quadrilateral area coordinate method (QACM-II). *International Journal for Numerical Methods in Engineering*, vol. 77, no. 8, pp. 1172–1200.

Chen, C.-N. (1999): The development of irregular elements for differential quadrature element method steady-state heat conduction analysis. *Computer Methods in Applied Mechanics and Engineering*, vol. 170, no. 1-2, pp. 1–14.

Chen, C.-N. (1999): The differential quadrature element method irregular element torsion analysis model. *Applied Mathematical Modelling*, vol. 23, no. 4, pp. 309–328.

Chen, C.-N. (2000): A generalized differential quadrature element method. *Computer Methods in Applied Mechanics and Engineering*, vol. 188, no. 1-3, pp. 553–566.

Chen, C.-N. (2003): DQEM and DQFDM for the analysis of composite two-dimensional elasticity problems. *Composite Structures*, vol. 59, no. 1, pp. 3–13.

Cook, R. (2001): *Concepts and applications of finite element analysis*. Wiley.

Dong, L.; Atluri, S. (2012): Development of 3D T-Trefftz Voronoi cell finite elements with/without spherical voids &/or elastic/rigid inclusions for micromechanical modeling of heterogeneous materials. *CMC: Computers, Materials, & Continua*, vol. 29, no. 2, pp. 169–211.

Dong, L.; Atluri, S. (2012): Development of 3D Trefftz Voronoi cell finite elements with ellipsoidal voids &/or elastic/rigid inclusions for micromechanical modeling of heterogeneous materials. *CMC: Computers, Materials, & Continua*, vol. 30, no. 1, pp. 39–81.

Dong, L.; Atluri, S. (2012): A simple multi-source-point T-Trefftz method for solving direct/inverse SHM problems of plane elasticity in arbitrary multiply-connected domains. *CMES - Computer Modeling in Engineering and Sciences*, vol. 85, no. 1, pp. 1–43.

Dong, L.; Atluri, S. (2012): T-Trefftz Voronoi cell finite elements with elastic/rigid inclusions or voids for micromechanical analysis of composite and porous materials. *CMES - Computer Modeling in Engineering and Sciences*, vol. 83, no. 2, pp. 183–219.

Dong, L.; Atluri, S. (2013): SGBEM Voronoi Cells (SVCs), with embedded arbitrary-shaped inclusions, voids, and/or cracks, for micromechanical modeling of heterogeneous materials. *CMC: Computers, Materials, & Continua*, vol. 33, no. 2, pp. 111–154.

Fantuzzi, N. (2013): *Generalized Differential Quadrature Finite Element Method applied to Advanced Structural Mechanics*. PhD thesis, University of Bologna, 2013.

Ferreira, A.; Viola, E.; Tornabene, F.; Fantuzzi, N.; Zenkour, A. (2013): Analysis of sandwich plates by generalized differential quadrature method. *Mathematical Problems in Engineering*, vol. 2013, pp. 1–12. Article ID 964367, doi:10.1155/2013/964367.

Ferretti, E. (2001): *Modellazione del Comportamento del Cilindro Fasciato in Compressione*. PhD thesis, Università del Salento, 2001.

Ferretti, E. (2003): Crack propagation modeling by remeshing using the Cell Method (CM). *CMES: Computer Modeling in Engineering & Sciences*, vol. 4, pp. 51–72.

Ferretti, E. (2004): A Cell Method (CM) code for modeling the pullout test step-wise. *CMES: Computer Modeling in Engineering & Sciences*, vol. 6, pp. 453–476.

Ferretti, E. (2004): Crack-path analysis for brittle and non-brittle cracks: A Cell Method approach. *CMES: Computer Modeling in Engineering & Sciences*, vol. 6, pp. 227–244.

Ferretti, E. (2004): A discrete nonlocal formulation using local constitutive laws. *International Journal of Fracture*, vol. 130, no. 3, pp. 175–182.

Ferretti, E. (2005): A local strictly nondecreasing material law for modeling softening and size-effect: a discrete approach. *CMES: Computer Modeling in Engineering & Sciences*, vol. 9, pp. 19–48.

Ferretti, E. (2009): Cell Method analysis of crack propagation in tensioned concrete plates. *CMES: Computer Modeling in Engineering & Sciences*, vol. 54, pp. 253–281.

Ferretti, E. (2012): Shape-effect in the effective law of plain and rubberized concrete. *CMC: Computers, Materials, & Continua*, vol. 30, pp. 237–284.

Ferretti, E. (2013): The Cell Method: an enriched description of physics starting from the algebraic formulation. *CMC: Computers, Materials, & Continua*, vol. 36, no. 1, pp. 49–72.

Ferretti, E. (2013): A Cell Method stress analysis in thin floor tiles subjected to temperature variation. *CMC: Computers, Materials, & Continua*, vol. 36, no. 3, pp. 293–322.

Ferretti, E. (2014): *The Cell Method: a purely algebraic computational method in physics and engineering science*. Momentum Press.

Ferretti, E.; Casadio, E.; Di Leo, A. (2008): Masonry walls under shear test: a CM modeling. *CMES: Computer Modeling in Engineering & Sciences*, vol. 30, pp. 163–190.

Gu, Y. T.; Liu, G. R. (2001): A Meshless Local Petrov-Galerkin (MLPG) method for free and forced vibration analyses for solids. *Computational Mechanics*, vol. 27, no. 3, pp. 188–198.

Han, Z. D.; Liu, H. T.; Rajendran, A. M.; Atluri, S. N. (2006): The applications of Meshless Local Petrov-Galerkin (MLPG) approaches in high-speed impact, penetration and perforation problems. *CMES - Computer Modeling in Engineering and Sciences*, vol. 14, no. 2, pp. 119–128.

Li, Q.; Shen, S.; Han, Z.; Atluri, S. (2003): Application of Meshless Local Petrov-Galerkin (MLPG) to problems with singularities, and material discontinuities, in 3-D elasticity. *CMES - Computer Modeling in Engineering and Sciences*, vol. 4, no. 5, pp. 571–585.

Li, S.; Atluri, S. N. (2008): The MLPG mixed collocation method for material orientation and topology optimization of anisotropic solids and structures. *CMES - Computer Modeling in Engineering and Sciences*, vol. 30, no. 1, pp. 37–56.

Li, S.; Atluri, S. N. (2008): Topology-optimization of structures based on the MLPG mixed collocation method. *CMES - Computer Modeling in Engineering and Sciences*, vol. 26, no. 1, pp. 61–74.

Li, Y.; Viola, E. (2013): Size effect investigation of a central interface crack between two bonded dissimilar materials. *Composite Structures*, vol. 105, pp. 90–107.

Liu, F.-L. (1999): Differential quadrature element method for static analysis of shear deformable cross-ply laminates. *International Journal for Numerical Methods in Engineering*, vol. 46, no. 8, pp. 1203–1219.

Macneal, R. H.; Harder, R. L. (1985): A proposed standard set of problems to test finite element accuracy. *Finite Elements in Analysis and Design*, vol. 1, no. 1, pp. 3–20.

Marzani, A.; Tornabene, F.; Viola, E. (2008): Nonconservative stability problems via generalized differential quadrature method. *Journal of Sound & Vibration*, vol. 315, no. 1-2, pp. 176–196.

Rezaiee-Pajand, M.; Karkon, M. (2013): An effective membrane element based on analytical solution. *European Journal of Mechanics - A/Solids*, vol. 39, pp. 268–279.

Shu, C. (2000): *Differential Quadrature and Its Applications in Engineering*. Springer Verlag.

Sladek, J.; Sladek, V.; Atluri, S. N. (2004): Meshless Local Petrov-Galerkin method for heat conduction problem in an anisotropic medium. *CMES - Computer Modeling in Engineering and Sciences*, vol. 6, no. 3, pp. 309–318.

Sod, G. A. (1978): A survey of several finite difference methods for systems of nonlinear hyperbolic conservation laws. *Journal of Computational Physics*, vol. 27, pp. 1–31.

Timoshenko, S. (1934): *Theory of Elasticity*. Engineering Societies Monographs. McGraw-Hill book Company, Incorporated.

Tonti, E. (2001): A direct discrete formulation of field laws: the Cell Method. *CMES: Computer Modeling in Engineering & Sciences*, vol. 2, pp. 237–258.

Tornabene, F. (2009): Free vibration analysis of functionally graded conical, cylindrical and annular shell structures with a four-parameter power-law distribution. *Computer Methods in Applied Mechanics and Engineering*, vol. 198, no. 37-40, pp. 2911–2935.

Tornabene, F. (2011): 2-D GDQ solution for free vibrations of anisotropic doubly-curved shells and panels of revolution. *Composite Structures*, vol. 93, pp. 1854–1876.

Tornabene, F. (2011): Free vibration of laminated composite doubly-curved shells and panels of revolution via GDQ method. *Computer Methods in Applied Mechanics and Engineering*, vol. 200, pp. 931–952.

Tornabene, F. (2011): Free vibrations of anisotropic doubly-curved shells and panels of revolution with a free-form meridian resting on Winkler-Pasternak elastic foundations. *Composite Structures*, vol. 94, pp. 186–206.

Tornabene, F. (2012): *Meccanica delle Strutture a Guscio in Materiale Composito. Il Metodo Generalizzato di Quadratura Differenziale*. Esculapio.

Tornabene, F.; Ceruti, A. (2013): Free-form laminated doubly-curved shells and panels of revolution on Winkler-Pasternak elastic foundations: A 2D GDQ solution for static and free vibration analysis. *World Journal of Mechanics*, vol. 3, pp. 1–25.

Tornabene, F.; Ceruti, A. (2013): Mixed static and dynamic optimizazion of four-parameter functionally graded completely doubly-curved and degenerate shells and panels using GDQ method. *Mathematical Problems in Engineering*, vol. 2013, pp. 1–33.

Tornabene, F.; Fantuzzi, N.; Viola, E.; Carrera, E. (2014): Static analysis of doubly-curved anisotropic shells and panels using CUF approach, differential geometry and differential quadrature method. *Composite Structures*, vol. 107, pp. 675–697.

Tornabene, F.; Fantuzzi, N.; Viola, E.; Cinefra, M.; Carrera, E.; Ferreira, A.; Zenkour, A. (2014): Analysis of thick isotropic and cross-ply laminated plates by generalized differential quadrature method and a unified formulation. *Composite Part B Engineering*. In Press.

Tornabene, F.; Fantuzzi, N.; Viola, E.; Ferreira, A. J. M. (2013): Radial basis function method applied to doubly-curved laminated composite shells and panels with a general higher-order equivalent single layer theory. *Composite Part B Engineering*, vol. 55, pp. 642–659.

Tornabene, F.; Fantuzzi, N.; Viola, E.; Reddy, J. (2014): Winkler-Pasternak foundation effect on the static and dynamic analyses of laminated doubly-curved and degenerate shells and panels. *Composite Part B Engineering*, vol. 57, pp. 269–296.

Tornabene, F.; Liverani, A.; Caligiana, G. (2011): FGM and laminated doubly-curved shells and panels of revolution with a free-form meridian: a 2-D GDQ solution for free vibrations. *International Journal of Mechanical Sciences*, vol. 53, pp. 446–470.

Tornabene, F.; Liverani, A.; Caligiana, G. (2012): General anisotropic doubly-curved shell theory: a differential quadrature solution for free vibrations of shells and panels of revolution with a free-form meridian. *Journal of Sound & Vibration*, vol. 331, pp. 4848–4869.

Tornabene, F.; Liverani, A.; Caligiana, G. (2012): Laminated composite rectangular and annular plates: a GDQ solution for static analysis with a posteriori shear and normal stress recovery. *Composite Part B Engineering*, vol. 43, pp. 1847–1872.

Tornabene, F.; Liverani, A.; Caligiana, G. (2012): Static analysis of laminated composite curved shells and panels of revolution with a posteriori shear and normal stress recovery using generalized differential quadrature method. *International Journal of Mechanical Sciences*, vol. 61, pp. 71–87.

Tornabene, F.; Marzani, A.; Viola, E.; Elishakoff, I. (2010): Critical flow speeds of pipes conveying fluid by the generalized differential quadrature method. *Advances in Theoretical and Applied Mechanics*, vol. 3, no. 3, pp. 121–138.

Tornabene, F.; Reddy, J. (2013): FGM and laminated doubly-curved and degenerate shells resting on nonlinear elastic foundation: a GDQ solution for static analysis with a posteriori stress and strain recovery. *Journal of Indian Institute of Science*. In Press.

Tornabene, F.; Viola, E. (2007): Vibration analysis of spherical structural elements using the GDQ method. *Computers & Mathematics with Applications*, vol. 53, no. 10, pp. 1538–1560.

Tornabene, F.; Viola, E. (2008): 2-D solution for free vibrations of parabolic shells using generalized differential quadrature method. *European Journal of Mechanics - A/Solids*, vol. 27, no. 6, pp. 1001–1025.

Tornabene, F.; Viola, E. (2009): Free vibration analysis of functionally graded panels and shells of revolution. *Meccanica*, vol. 44, no. 3, pp. 255–281.

Tornabene, F.; Viola, E. (2009): Free vibrations of four-parameter functionally graded parabolic panels and shell of revolution. *European Journal of Mechanics - A/Solids*, vol. 28, no. 5, pp. 991–1013.

Tornabene, F.; Viola, E. (2013): Static analysis of functionally graded doubly-curved shells and panels of revolution. *Meccanica*, vol. 48, pp. 901–930.

Tornabene, F.; Viola, E.; Fantuzzi, N. (2013): General higher-order equivalent single layer theory for free vibrations of doubly-curved laminated composite shells and panels. *Composite Structures*, vol. 104, pp. 94–117.

Tornabene, F.; Viola, E.; Inman, D. J. (2009): 2-D differential quadrature solution for vibration analysis of functionally graded conical, cylindrical and annular shell structures. *Journal of Sound & Vibration*, vol. 328, no. 3, pp. 259–290.

Viola, E.; Dilena, M.; Tornabene, F. (2007): Analytical and numerical results for vibration analysis of multi-stepped and multi-damaged circular arches. *Journal of Sound & Vibration*, vol. 299, no. 1-2, pp. 143–163.

Viola, E.; Rossetti, L.; Fantuzzi, N. (2012): Numerical investigation of functionally graded cylindrical shells and panels using the generalized unconstrained third order theory coupled with the stress recovery. *Composite Structures*, vol. 94, pp. 3736–3758.

Viola, E.; Tornabene, F. (2005): Vibration analysis of damaged circular arches with varying cross-section. *Structural Integrity & Durability (SID-SDHM)*, vol. 1, no. 2, pp. 155–169.

Viola, E.; Tornabene, F. (2006): Vibration analysis of conical shell structures using GDQ method. *Far East Journal of Applied Mathematics*, vol. 25, no. 1, pp. 23–39.

Viola, E.; Tornabene, F. (2009): Free vibrations of three parameter functionally graded parabolic panels of revolution. *Mechanics Research Communications*, vol. 36, no. 5, pp. 587–594.

Viola, E.; Tornabene, F.; Fantuzzi, N. (2013): General higher-order shear deformation theories for the free vibration analysis of completely doubly-curved laminated shells and panels. *Composite Structures*, vol. 95, pp. 639–666.

Viola, E.; Tornabene, F.; Fantuzzi, N. (2013): Generalized differential quadrature finite element method for cracked composite structures of arbitrary shape. *Composite Structures*, vol. 106, pp. 815–834.

Viola, E.; Tornabene, F.; Fantuzzi, N. (2013): Static analysis of completely doubly-curved laminated shells and panels using general higher-order shear deformation theories. *Composite Structures*, vol. 101, pp. 59–93.

Wu, C.; Guo, Y.; Askari, E. (2013): Numerical modeling of composite solids using an immersed meshfree Galerkin method. *Composites Part B: Engineering*, vol. 45, no. 1, pp. 1397–1413.

Wu, C. T.; Park, C. K.; Chen, J. S. (2011): A generalized approximation for the meshfree analysis of solids. *International Journal for Numerical Methods in Engineering*, vol. 85, no. 6, pp. 693–722.

Xing, Y.; Liu, B. (2009): High-accuracy differential quadrature finite element method and its application to free vibrations of thin plate with curvilinear domain. *International Journal for Numerical Methods in Engineering*, vol. 80, no. 13, pp. 1718–1742.

Xing, Y.; Liu, B.; Liu, G. (2010): A differential quadrature finite element method. *International Journal of Applied Mechanics*, vol. 2, pp. 207–227.

Yuqiu, L.; Yin, X. (1994): Generalized conforming triangular membrane element with vertex rigid rotational freedoms. *Finite Elements in Analysis and Design*, vol. 17, no. 4, pp. 259–271.

Zhong, H.; He, Y. (1998): Solution of Poisson and Laplace equations by quadrilateral quadrature element. *International Journal of Solids and Structures*, vol. 35, no. 21, pp. 2805–2819.

Zhong, H.; Yu, T. (2009): A weak form quadrature element method for plane elasticity problems. *Applied Mathematical Modelling*, vol. 33, no. 10, pp. 3801–3814.

Zong, Z.; Lam, K.; Zhang, Y. (2005): A multidomain differential quadrature approach to plane elastic problems with material discontinuity. *Mathematical and Computer Modelling*, vol. 41, no. 4-5, pp. 539–553.

Zong, Z.; Zhang, Y. (2009): *Advanced Differential Quadrature Methods*. Chapman & Hall/CRC Applied Mathematics & Nonlinear Science. Taylor & Francis.